scientific reports

Check for updates

OPEN

Evaluation and optimal width ratio selection of microbial mineralization technique in the repair of lining cracks in Xinjiang desert open channel

Jianxin Wang[1,2]✉, Jianing Zhu[1], Yusheng Li[1], Shihao Zhang[1] & Chengming Feng[1]

The bank slope structure of the open channel in the Xinjiang desert is affected by seasonal climate changes and water erosion, leading to lining cracking. This study identified the optimal culture conditions and mineralization factors for Sporosarcina pasteurii through strain cultivation and precipitation assays. Subsequently, 0.1~5.0 mm wide penetrating concrete cracks were prefabricated, and microbially induced calcium carbonate precipitation (MICP) repair tests were conducted over 16 cycles. These experiments included macroscopic performance evaluations, such as area repair rate, penetration resistance, and capillary water absorption tests, alongside microscopic analyses using X-ray diffraction and scanning electron microscopy. The results indicate that MICP technology effectively repairs narrow cracks, preserving crack surface integrity, significantly reducing permeability and water absorption, and enhancing the durability of the concrete. However, for cracks exceeding 1.0 mm in width, the repair efficiency declines progressively. Based on the experimental data, it is concluded that a crack width of 1.0 mm is the optimal threshold for effective MICP-based repair within 16 cycles, ensuring both structural integrity and optimal waterproofing. These results offer valuable insights into the potential application of MICP technology for the remediation of lining cracks in the bank slopes of water conveyance channels in Xinjiang Desert.

Keywords Xinjiang desert open channel, MICP, Concrete lining crack repair, Crack width optimization, Macro–micro characterization

The bank slope of Xinjiang Desert Open Channel is subject to significant seasonal variations, which result in cyclical changes in temperature and canal water levels. Consequently, the impermeable lining layer undergoes prolonged alternating cycles of drying and wetting, as well as freezing and thawing. These conditions render the lining susceptible to erosion and cracking, thereby decreasing its permeability and durability. The most severe damage to the bank slope lining manifests as structural cracks, allowing canal water to infiltrate the aeolian soil. This infiltration fills the internal pores of the soil with water, eliminating the presence of a free liquid surface and consequently reducing the surface tension of the water. As a result, the cohesion within the aeolian soil is compromised, leading to potential landslide collapses of the bank slope, which adversely affects the normal operation of the desert channel. Therefore, the implementation of effective concrete lining crack repair technologies is crucial for ensuring the long-term functionality, safety, and stability of desert open channels.

Presently, the methods employed for the repair of concrete cracks primarily encompass epoxy resin injection, filling, grouting, and electrodeposition[1,2]. While these techniques have demonstrated effective reinforcement results, they exhibit certain limitations regarding energy consumption, compatibility, and environmental sustainability[3,4]. In recent years, microbially induced calcium carbonate precipitation (MICP) technology has received extensive attention as a novel reinforcement method. This technology promotes calcium carbonate precipitation through microbial metabolism, thereby achieving reinforcement and repair of materials. Its energy-saving, environmentally friendly, and low-interference characteristics make it show great potential in various application scenarios[5–7]. In special environments such as deserts, the adaptability of MICP technology is

[1]College of Hydraulic and Civil Engineering, Xinjiang Agricultural University, Urumqi 830052, China. [2]Xinjiang Key Laboratory of Hydraulic Engineering Security and Water Disasters Prevention, Urumqi 830052, China. ✉email: wangjianxin_wjx@163.com

also prominent. Miao et al.[8] and Meng et al.[9] carried out in-situ MICP sand-fixing experiments in the Tengger Desert and the Ulan Buh Desert, respectively. These experiments significantly improved the bearing capacity and erosion resistance of the surface soil and also achieved remarkable results in long-term durability assessments. These studies provide strong support for the application of MICP technology in high-temperature and drought environments such as deserts. At the same time, MICP technology also shows good application prospects in the field of concrete repair. Currently, numerous scholars, both domestically and internationally, have conducted extensive research on the application of MICP for concrete repair. Tittelboom et al.[10], Muynck et al.[11], Cuthbert et al.[12], and Khaliq et al.[13] indicated that under appropriate environmental conditions, Bacillus subtilis can generate CO_3^2 through its metabolic activities. This ion subsequently interacts with Ca^{2+} present in the surrounding environment, leading to the formation of biogenic $CaCO_3$ through a series of biochemical reactions. This process contributes to the repair of concrete cracks (Fig. 1). Furthermore, electron microscopy analyses reveal that the calcite product exhibits favorable compatibility with the concrete matrix, thereby facilitating a sustainable repair effect. The calcite produced demonstrates significant compatibility with the concrete matrix, enabling ongoing repair capabilities[14,15].

Currently, Jiang[16] conducted a comparative analysis of the advantages and challenges associated with MICP passive repair and active self-repairing concrete, as well as potential solutions to these challenges. MICP self-healing technology pre-implants microorganisms and nutrients in concrete, enabling the repair process to start automatically when cracks occur. This technology boasts several advantages, such as strong repair continuity, excellent.

repair effects on small cracks, and the ability to achieve long-term self-maintenance of the concrete structure. However, it also has notable drawbacks, including a long repair cycle, limited repair capacity for cracks (usually up to 400~500 μm), difficulty in ensuring the long-term activity of microorganisms, and high initial preparation costs[17–21]. In contrast, MICP passive repair involves injecting microorganisms and reaction fluids into cracks after they appear. This method offers operational flexibility and can be tailored to different crack sizes at relatively low costs. Nevertheless, it requires manual intervention, resulting in poor repair timeliness, and the stability of its repair effect in complex environments remains to be further verified. Choi[22] employed the immersion method for 21 cycles of MICP repair on mortar cracks with widths varying from 0.15 to 1.64 mm, resulting in a reduction of the permeability coefficients of the specimens by approximately three orders of magnitude. Tittelboom et al.[10] investigated the water permeability of MICP-repaired concrete using the immersion method on splitting cracks with average widths ranging from 0.05 to 0.87 mm. Their water permeability tests revealed a significant reduction in the water permeability of the repaired concrete, with a significant trend of decreasing permeability correlating with the reduction of initial crack widths. Jongvivatsakul et al.[23] repaired mortar cracks measuring 0.4 mm in width over a period of 20 d, revealing that the water absorption rate of the specimens repaired via MICP was 7.2×10^{-6} m/s$^{1/2}$, approximately 72% lower than that of the cracked specimens. Given that the focus of this study is on the repair of bank slope lining cracks in the constructed Xinjiang Desert Water Open Channel, the investigation of MICP active self-repairing methods is not addressed at this time. Instead, the primary emphasis is placed on the research of MICP passive repair of existing lining cracks. Additionally, the applicability of the immersion method for repair has been found to be limited by numerous scholars. Therefore, the injection method is employed for MICP repair of desert channel lining cracks. Huang et al.[24], Lu et al.[4], and Jia et al.[25] utilized the steel plate insertion and extraction method to prefabricate concrete cracks of specific widths, which were repaired using MICP and then a series of macro–micro experiments were conducted to

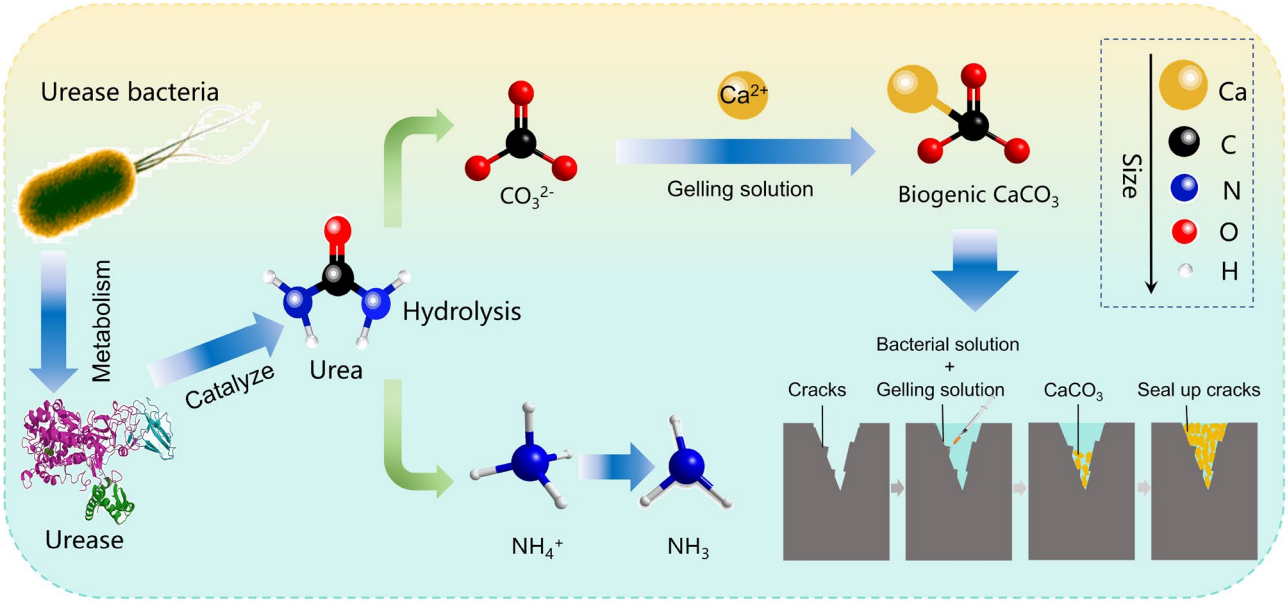

Fig. 1. Mechanism of microbial mineralization for repair of concrete cracks.

evaluate the repair performance. Their research not only focused on the improvement of impermeability after MICP crack repair but also explored the impact of MICP on the compressive strength of concrete. The study indicated that the enhancement of compressive strength by MICP was relatively limited, typically increasing by only 3% to 7%. This phenomenon is mainly attributed to the fact that MICP repair relies on calcium carbonate precipitation to fill cracks rather than directly reinforcing the overall structural strength of the concrete matrix. Therefore, in crack repair research, the primary function of MICP is to improve impermeability and durability rather than significantly enhancing compressive strength.

The aforementioned research indicates that significant developments have been made by scholars both domestically and internationally in the area of MICP for the repair of concrete cracks. Current studies primarily focus on validating the feasibility of MICP as a method for repairing concrete cracks. Given that the lining of the bank slope in Xinjiang desert open channel is affected by multiple factors such as seasonal climate changes, alternating wetting and drying, and freezing and thawing, the depth and width of the lining cracks exhibit complex and irregular distribution characteristics. There are significant differences in the crack dimensions and orientations under natural conditions. Therefore, it is highly challenging to conduct in-situ comparative experiments directly. Therefore, this study utilized cylindrical specimens measuring 10 cm in diameter and 6 cm in height (with a lining thickness of 6 cm), which were prefabricated based on the the thickness and strength of the bank slope lining of Gurbantunggut Desert Open Channel in Xinjiang. Subsequently, regular structural cracks of 5.0 cm in length and 0.1 mm to 5.0 mm in width were intentionally created using a steel-plate insertion and extraction technique to simulate their most hazardous conditions. MICP repair tests were performed using the injection method, with a total of 16 cycles, once a day, for a total of 16 times. The specimens were then subjected to MICP repairs, and evaluations were performed under varying crack widths and repair durations. The effectiveness of MICP technology in repairing cracks was assessed by macroscopic tests such as measure the apparent crack area repair rate, impermeability, and waterproofing performance of the specimens across different widths and repair periods, combined with microscopic tests such as XRD mineral diffraction tests and SEM scanning electron microscopy tests. The research results provide valuable insights into the application of MICP technology for the repair of cracks in the bank slope lining of water conveyance channels in Xinjiang Desert, ultimately establishing a optimal width ($Width_0$) threshold for effective crack repair within a specified repair cycle.

Test materials and test schemes

Microbial selection and culture

Microbe stain cultivating

Sporosarcina pasteurii (ATCC 11859) was utilized in the concrete crack repair experiment, purchased from the Shanghai Microbiology Conservation Center, China. Firstly, the strain medium was prepared according to the medium formula, which consisted of 1 L of ultrapure water, 20 g of yeast extract, 15 g of NH_4Cl, 12 mg of $MnSO_4{\cdot}H_2O$, 24 mg of $NiCl_2{\cdot}6H_2O$, and 15 g of agar to create a solid medium[5,6]. Then the medium was prepared and put into autoclave using 121℃ autoclave sterilization for 20 min, and then placed on the ultra-clean bench for cooling; Finally, the microbial lyophilized powder was activated for inoculation and passaging, and after inoculation, it was transferred to the oscillator and cultured at 200 rpm for 24 h, and then the activity of the strain could be determined.

Test conditions

The bacterial strains were incubated under various controlled conditions, resulting in an increase in their activity over time. The change in conductivity of the urea solution was measured at the 5-min mark using a conductivity method, which assessed the ability of urease to hydrolyze urea. This measurement was employed to characterize the urease activity of the bacterial solution[26].

$$\text{Conductivity}\,(\text{ms/min}) = \frac{\text{EC}_{5\text{min}} - \text{EC}_{\text{initial}}}{5} \tag{1}$$

where $EC_{initial}$, EC_{5min} are the initial conductivity (ms/cm), conductivity after 5 min (ms/cm), respectively.

In this study, an orthogonal experimental design was employed to evaluate the comprehensive effects of multiple factors on microbial cultivation and the mineralization process. Initially, nine experimental combinations were conducted for microbial suspensions under different culture conditions (pH, temperature, mother liquor, and culture solution content), with each factor at three different levels. The impact of different factor combinations on microbial activity was assessed through range analysis and Spearman correlation analysis. Microbial activity was measured using electrical conductivity tests to determine the optimal growth and reproduction conditions for the strains.

Based on the optimal culture conditions for the strains, further experiments were conducted using a three-factor (bacterium-to-gel ratio, type of calcium source, and calcium ion concentration) and four-level design, comprising 16 experimental combinations. These experiments aimed to identify the mineralization factors influencing microbial-induced calcium carbonate precipitation (MICP). The comprehensive effects of different factor combinations on the mineralization process were evaluated using range analysis and Spearman correlation analysis, and the optimal MICP mineralization conditions were determined. The control indicators for strain culture conditions and mineralization effect conditions are presented in Table 1.

Cracked concrete specimen fabrication

The cement utilized is ordinary silicate cement. The fine aggregate consists of natural river sand with a fineness modulus of 2.7, while the coarse aggregate is gravel with a grain size ranging from 5 to 20 mm. The mixing water

Strain growth and reproduction conditions				Factors affecting bacterial mineralization		
pH	Temperature (℃)	Mother liquor (mL)	Cement (mL)	Bacterial gel ratio	Type of calcium source	Calcium concentration (mol/L)
8	25	1.0	100	1:0.5	Calcium chloride	0.5
9	30	1.5	150	1:1	Calcium acetate	1.0
				1:1.5	Calcium nitrate	1.5
10	35	2.0	200	1:2	Calcium lactate	2.0

Table 1. Indicators of strain culture and mineralization control.

ID	Repair method	Crack width/mm	Area restoration rate	Penetration test	Capillary water absorption test	SEM XRD	Restoration measures	Number of specimens
1	MICP	0.1, 0.2, 0.3, 0.4	√	√	√	√	Injection	120
		0.5, 0.8, 1.0, 1.5						
		2.0, 2.5, 3.0, 4.0						
		5.0						

Table 2. Experimental program for MICP repair of concrete cracks. For each type of crack, three sets of specimens are prepared and the average value is taken as the test result.

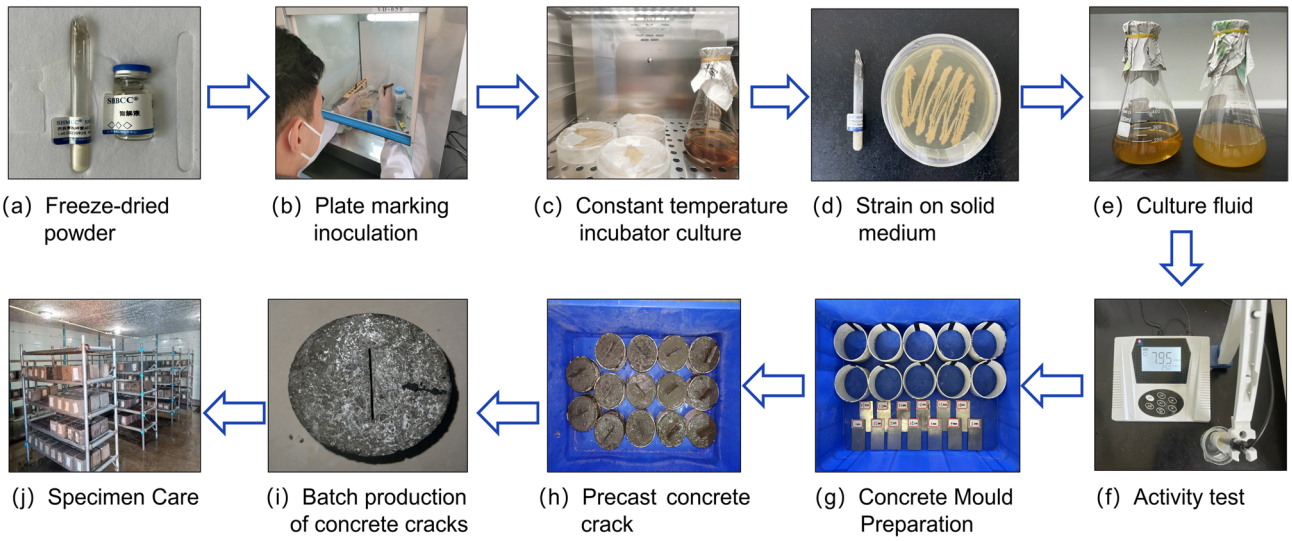

Fig. 2. Preparation process of microbial concrete.

employed is tap water. The designed strength grade of the concrete was C20 based on the strength of the lining of the bank slope of the desert open channel[27,28].

In the study of microbial mineralization restoration, according to the thickness of the bank slope lining is 6 cm, a concrete cylinder with dimensions of Φ100 mm × 60 mm was utilized, featuring crack lengths and depths of 50 mm and 60 mm, respectively, with crack widths ranging from 0.1 to 5.0 mm, 120 test pieces in total. To achieve the desired crack parameters (e.g., length, depth, and width) steel plate insertion and extraction techniques were employed to create the corresponding pre-fabricated cracks during the fabrication of the concrete cylinder specimens, the specific crack widths are detailed in Table 2.

To prevent adhesion between the steel component and the concrete, and to facilitate the smooth extraction of the steel component, it is recommended to apply a thin layer of lubricating oil to the surface of the steel prior to the concrete pouring process. After a duration of 16~18 h post-pouring, the steel component was gradually removed from the concrete to minimize the risk of damaging the surface of the resulting crack. The cracks exhibited a simple and clear appearance following the extraction of the steel components, as this procedure was conducted after the concrete had reached its final setting. Subsequently, the cracked specimens were subjected to a curing process in a standard curing box for a period of 28 d, after which the subsequent phase of the crack repair testing was initiated. The preparation process for the microbial repair concrete crack specimens is illustrated in Fig. 2.

Rehabilitation assessment program

The cracks were treated using MICP over a duration of 16 d. During this period, the area repair rate, permeability coefficient recovery rate and capillary water absorption recovery rate of concrete specimens with different crack widths and repair time were observed. This evaluation aimed to assess the effectiveness of MICP in addressing the cracks in the nullah lining and to compare the selected Width0. The various concrete crack repair options are summarized in Table 2, while the repair process is depicted in Fig. 3A.

Macro performance testing

(a) Area restoration rate

The variations in the overall width of the cracks on the specimen surface were documented using a camera. Daily recordings of the cracks on the specimen surface were made both prior to and following the repair process. Image binarization was subsequently applied to quantify the number of pixels in the area before and after the crack repair (Fig. 3B(a))[29], 39 specimens in total. The overall area repair rate of cracks of varying widths over a period of 16 d was calculated through Eq. 4. A three-dimensional fitting surface was constructed with X–Y-Z axes representing crack width, repair duration, and area repair rate. This fitting formula was developed to serve as a reference for the area repair of cracks in desert channel linings;

(b) Penetration test

The variation in water penetration before and after the repair of cracks in concrete specimens indicates that the recovery rate of permeability coefficient can serve as a quantitative measure of the effectiveness of crack repair, with a total of 39 specimens tested. During the repair and curing of the specimens, permeability tests were conducted both before and after the repair. In the test, the concrete sample is connected to a polyvinyl chloride (PVC) pipe, which has a diameter of 100 mm and a length of 1200 mm. The top of the pipe is equipped with a water level inlet and outlet to maintain a constant water head height of 1.0 m within the PVC pipe. Before the test, the connection between the concrete specimen and the PVC pipe is tightly sealed with epoxy resin to prevent water leakage. The constant head permeability test is carried out to measure the amount of water permeated in a constant time, and the permeability coefficient of each group of samples is determined before and after repair using Darcy's law. The test setup is shown in Fig. 3B(b). The permeability coefficient (k_s) for each group of specimens was determined using Eq. 2[11].

$$k_s = \frac{Q \cdot L}{A \cdot t \cdot \Delta h} \tag{2}$$

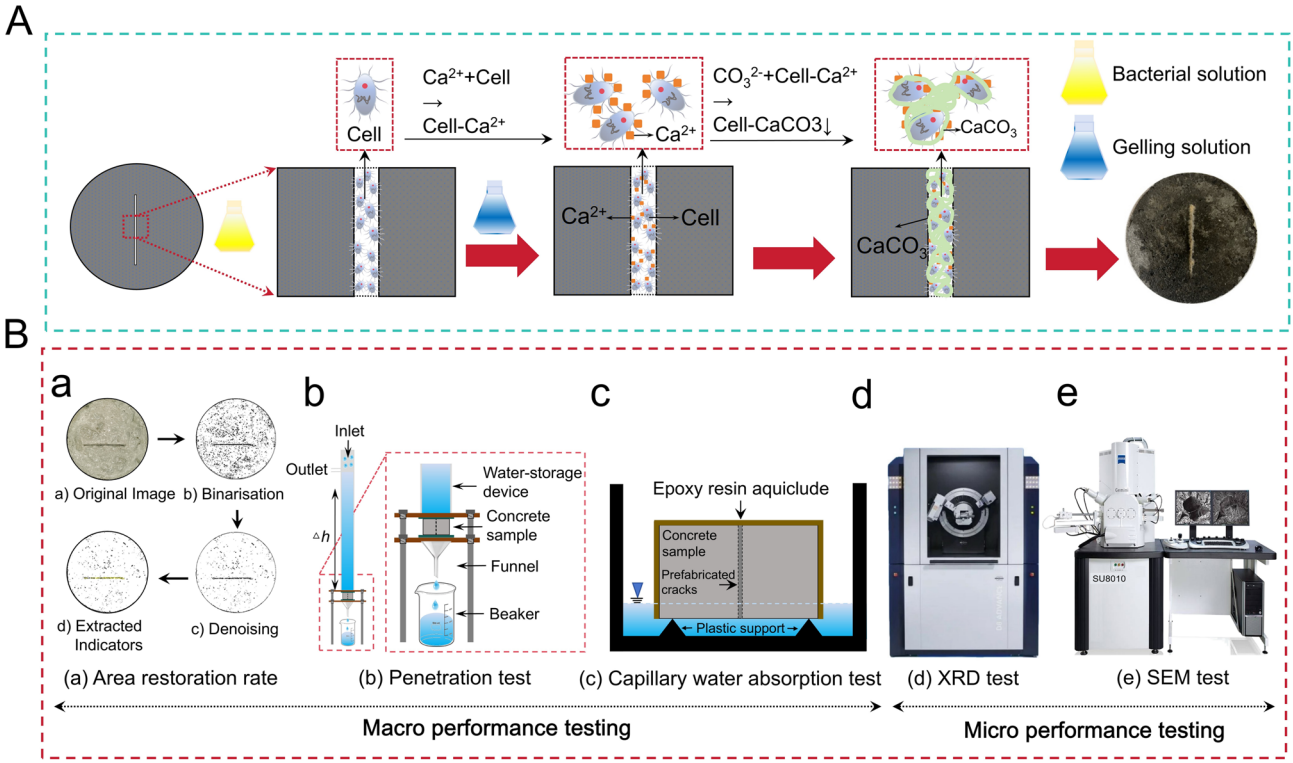

Fig. 3. Microbial repair of concrete cracks process and test.

where k_s is the permeability coefficient of the specimen, cm/s; Q is the seepage quantity, mL; L is the thickness of the specimen, cm, A is the surface area of the specimen, cm^2, t is the penetration time, s and Δh is the difference in head, cm.

The rates of recovery in the permeability coefficient of concrete cracks, characterized by varying widths and durations, were computed in accordance with Eq. 4 as a reference for the anti-seepage repair of cracks in desert channel linings;

(c) Capillary water absorption test

The concrete specimens were placed in a blast drying oven at a temperature of 105 ± 5 °C, dried for 24 h and cooled to room temperature. In order to achieve the effect of one-sided water absorption of the concrete specimens, the sides and top of the cooled cylindrical concrete specimens were sealed with aluminum foil tape, and the mass of the specimens was weighed after the sealing was completed and recorded as m_0; the repaired surface was placed in the water face down and supported by a bracket, and the test setup was schematically shown in Fig. 3B(c), 42 specimens in total. The mass m after water absorption was weighed periodically for a total of 48 h. The water absorption of the cylindrical concrete specimens can be reflected by the one-dimensional cumulative capillary absorption height of the specimens, and the one-dimensional cumulative capillary absorption height of the specimens, i (mm)[30], can be calculated according to Eq. 3[31], and the waterproofing performance enhancement rate of the concrete specimens after the MICP repairs was calculated by Eq. 4.

$$i = \frac{m - m_0}{A \cdot \rho_\omega} \tag{3}$$

where m_0, m is the mass of the concrete specimen when dry and after immersion in water, respectively, g; A is the surface area of the specimen, mm^2, and ρ_ω is the density of water, g/mm^3.

In summary (a-c), the area repair rate λ_s, permeability coefficient recovery rate λ_k, and capillary water absorption recovery rate λ_w of the repaired concrete were used to characterize the MICP repair effect, in which the lifting coefficient λ was uniformly calculated according to the following formula:

$$\lambda = \left| \frac{p_r - p_u}{p_0 - p_u} \right| \times 100\% \tag{4}$$

where p_0, p_r and p_u represent the performance parameters of the intact specimen, the repaired specimen, and the unrepaired specimen, respectively. Specifically, p_0 is directly measured from the intact specimen (e.g., the permeability coefficient k_0 and the capillary rise height i_0); p_u represents the baseline value of the cracked specimen without repair (e.g., k_u and i_u); and p_r is the measured value after MICP repair (e.g., k_r and i_r). The parameter λ quantifies the contribution of MICP technology to crack repair by comparing the performance differences before and after the repair.

Micro performance testing

X-ray diffraction (XRD) was used to compare the composition of the material in the cracks of the specimens before and after repair, in which the XRD analysis was carried out at a 2θ angle ranging from 20° to 70°, with a step size of 0.02°, and a dwell time of 1 s for each step, to ensure that all possible diffraction data from the samples could be captured. Physical phase searches were performed using MDI JADE 6 to determine the resulting phase based on the three strong peak positions, peak intensities, and elements in the sample[24]. Additionally, the morphology of the products located within the cracks was comparatively examined using scanning electron microscopy (SEM), in which the accelerating voltage was 5.0 kV, the thickness of the spray coating was about 10 nm, and the slow scanning and selective area filming were carried out by adjusting the working distance (WD) and selecting the appropriate magnification[32], as presented in Fig. 3B(d).

Effect of MICP in repairing concrete cracks of different widths

Factors affecting strain culture and mineralization

Figure 4 depicts the dynamics of microbial urease activity across various strains under differing conditions, as well as the resultant effects on $CaCO_3$ precipitation. Figure 4a depicts the methodology employed to assess the urease activity of the strains, which is determined by measuring the change in conductivity at 25 °C over a duration of 5 min. Based on the growth and propagation conditions outlined in Table 1, an orthogonal test was conducted alongside Spearman's correlation analysis to ascertain the effect of varying incubation temperatures (°C), pH levels, mother liquor volumes (mL), and culture solution volumes (mL) on urease activity and their intercorrelations. The results of this research are presented in Fig. 4b,c. As the incubation temperature (CT) was increased from 25 to 35 °C, urease activity initially increased before subsequently declining, exhibiting a correlation coefficient (r) of – 0.42. Notably, 30 °C emerged as the critical threshold for urease activity, suggesting that an optimal temperature enhances the thermodynamic properties of the enzyme, thereby accelerating the catalytic reaction rate[33]. Conversely, excessively high temperatures can induce thermal denaturation of the enzyme structure, leading to a reduction in catalytic efficiency. Furthermore, the pH value set at 9 and the mother liquor volume (BLC) of 1.5 mL were found to significantly enhance the stability and activity of the enzyme, underscoring the critical role of acid–base balance and nutrient availability in the microbial growth environment[34,35]. Additionally, the optimal urease activity was observed at a culture medium volume of 100 mL, which mitigated diffusion limitations and optimized the contact efficiency between the substrate and the enzyme. This enhancement facilitated the exchange of metabolites and interactions among the strains, thereby

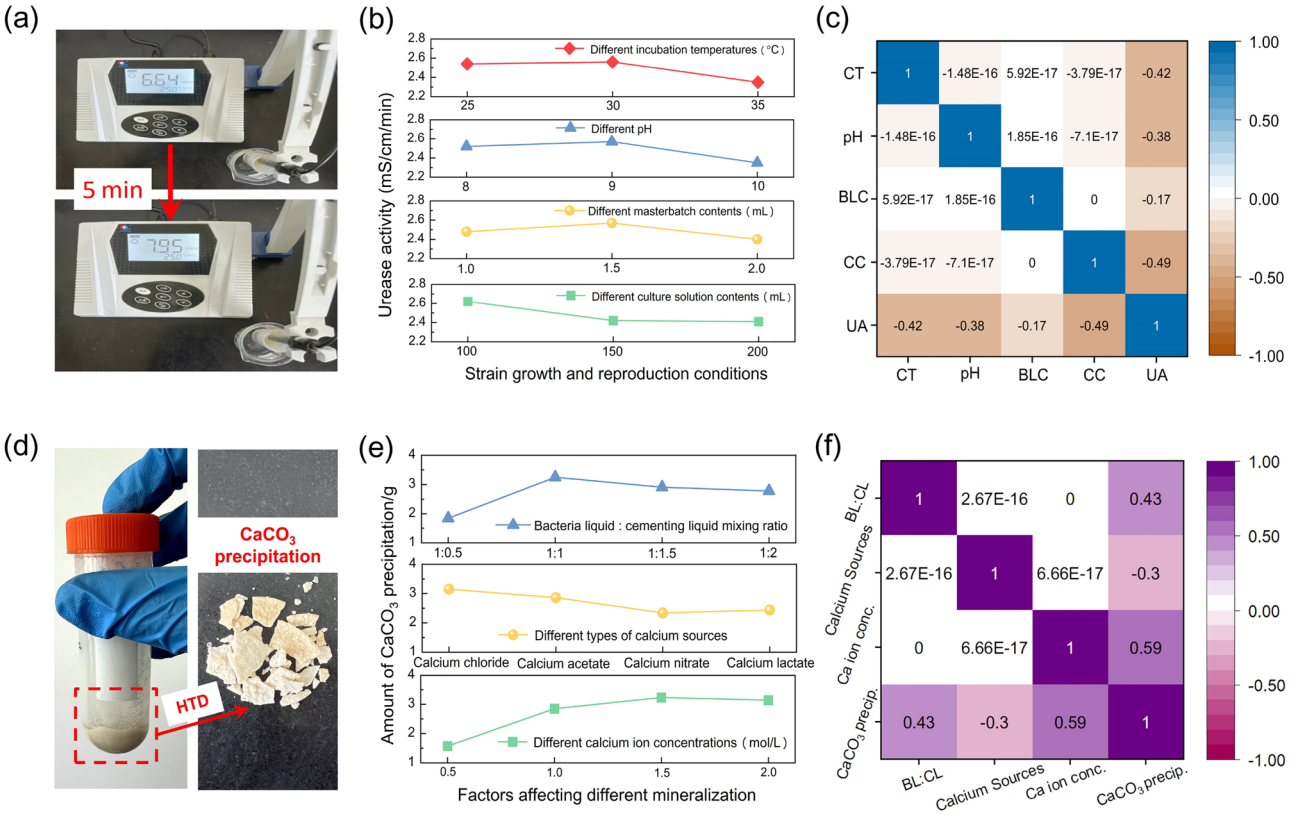

Fig. 4. Effect of mineralized environment of microbial culture on strain activity and sedimentation.

further improving urease catalytic efficiency through the reduction of diffusion constraints and the optimization of substrate-enzyme interactions[36,37].

From the aforementioned study regarding the factors affecting the growth and propagation of bacterial strains, the urease activity of these strains was optimal at a temperature of 30 °C, a pH value of 9, a mother liquor volume of 1.5 mL, and a culture solution volume of 100 mL. Under these conditions, the precipitation of $CaCO_3$, which is central to the mineralization process of MICP, was significantly enhanced. This study conducted a comprehensive analysis of the regulatory mechanisms associated with the bacterial gel ratio (BL:CL), Calcium Sources, and the concentration of Ca^{2+} (Ca ion conc.) on the extent of precipitation (Fig. 4d,e). The results indicated that as BL:CL ratio increased from 1:0.5 to 1:2, the amount of $CaCO_3$ precipitation initially increased and subsequently decreased, exhibiting r of 0.43. The rate of change in precipitation when BL:CL ratio increased from 1:0.5 to 1:1 was greater than that observed when the ratio increased from 1:1 to 1:2. By establishing a BL:CL ratio of 1:1 as the mineralization factor, $CaCO_3$ precipitation reached an equilibrium peak, wherein the microorganisms facilitated optimal conditions for attachment and metabolic activity, thereby promoting urease synthesis and $CaCO_3$ deposition. Furthermore, a comparison of various Ca sources revealed that $CaCl_2$ served as a more effective source of Ca^{2+} due to its high solubility, which expedited $CaCO_3$ precipitation process[38,39]. Ultimately, the most favorable precipitation effect was achieved at a Ca^{2+} concentration of 1.5 mol/L, which facilitated sufficient ionic reactions while mitigating the risk of excessive concentration that could inhibit precipitation[40].

Surface analysis of MICP repaired crack

The implementation of MICP repairs has led to the continuous generation and gradual accumulation of white precipitates within the cracks, ultimately facilitating the sealing of these fissures. To establish $Width_0$ for concrete crack repair only through MICP, a series of 16 consecutive cycles of MICP repair were conducted on concrete cracks with widths varying from 0.1 to 5.0 mm.

The area repair rate test was conducted initially, with the repair of certain specimens exhibiting width cracks in Fig. 5.

Figures 5 and 6a,b indicates that during MICP repair process, a light yellow precipitate accumulates progressively from the bottom of the crack. Notably, for cracks with widths less than 0.8 mm, there is minimal accumulation of the light yellow precipitate during the first four cycles. This phenomenon can be primarily attributed to the effect of gravity, which causes $CaCO_3$ precipitate to first settle at the bottom of the crack. Subsequently, it expands along the interior of the crack through adsorption effects before gradually rising[41].

Analysis in Fig. 7 reveals that for concrete cracks measuring between 0.1 and 0.8 mm in width, an area repair rate approaching 100% was achieved after 16 cycles, indicating effective crack sealing. However, as the

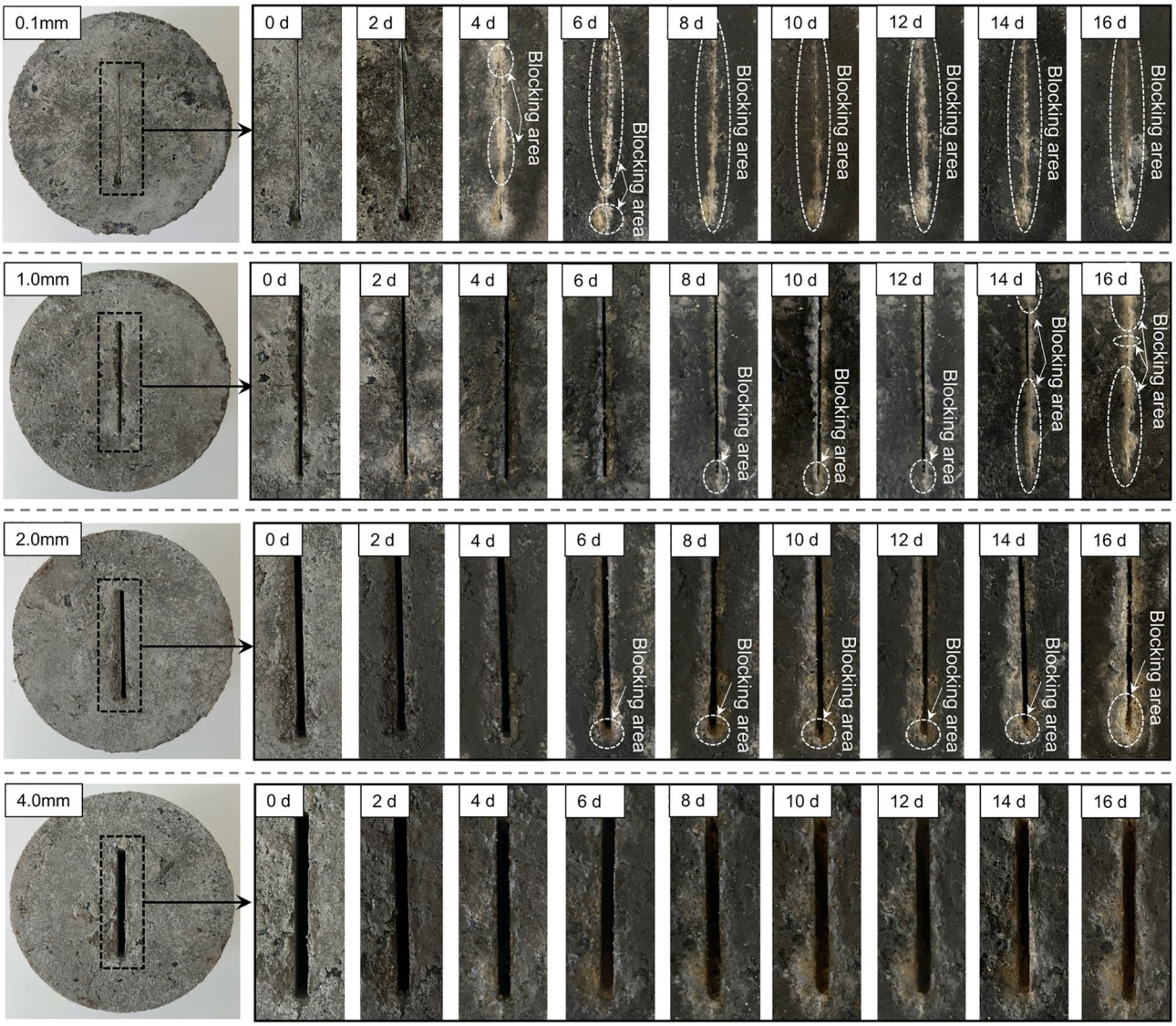

Fig. 5. Apparent condition of typical width cracks at 16 cycles.

crack width increased to 1.0 mm and beyond, the repair efficiency exhibited a significant decline. Specifically, the repair rate for 1.0 mm wide cracks decreased to 93.6% after 16 cycles, while the repair rate for 1.5 mm wide cracks was only 43.2%. This trend became increasingly pronounced as the crack width exceeded 1.5 mm, with the repair rate plummeting to less than 10%. This observation suggests that MICP technology has a limited capacity to repair wider cracks within 16 cycles. The decrease of remediation effect can be attributed to the hindered transport of microorganisms and their metabolites resulting from the increased crack width, as well as the physical constraints on the formation and accumulation of $CaCO_3$ precipitates, which adversely affect the restoration of the repair area.

Based on the experimental data presented, this study examines the relationship between crack width (w) and repair duration (t) in relation to the area repair rate. Utilizing surface fitting techniques, the intrinsic relationship among varying crack widths, repair durations, and the area repair rate following microbial mineralization repair was established. The fitting results are shown in Fig. 8 and Eq. 5. R^2 between the fitted results and the observed values.

is 0.89, indicating a strong fit. Therefore, Eq. 5 can serve as a surface model for the area repair rate of concrete cracks repaired through MICP.

$$\lambda_s = \frac{1.2}{\left[1+\left(\frac{-w}{0.827}\right)^{-3.19}\right]\left[1+\left(\frac{-t}{5.35}\right)^{-3.16}\right]} - 0.0213(R^2 = 0.89) \tag{5}$$

where λ_k is the area repair rate; w: crack width, mm; t: repair time, day. (**Note:** when the area repair rate of the fitted surface corresponding to different widths/repair days is less than 0, i.e., the area repair rate is taken to be 0;

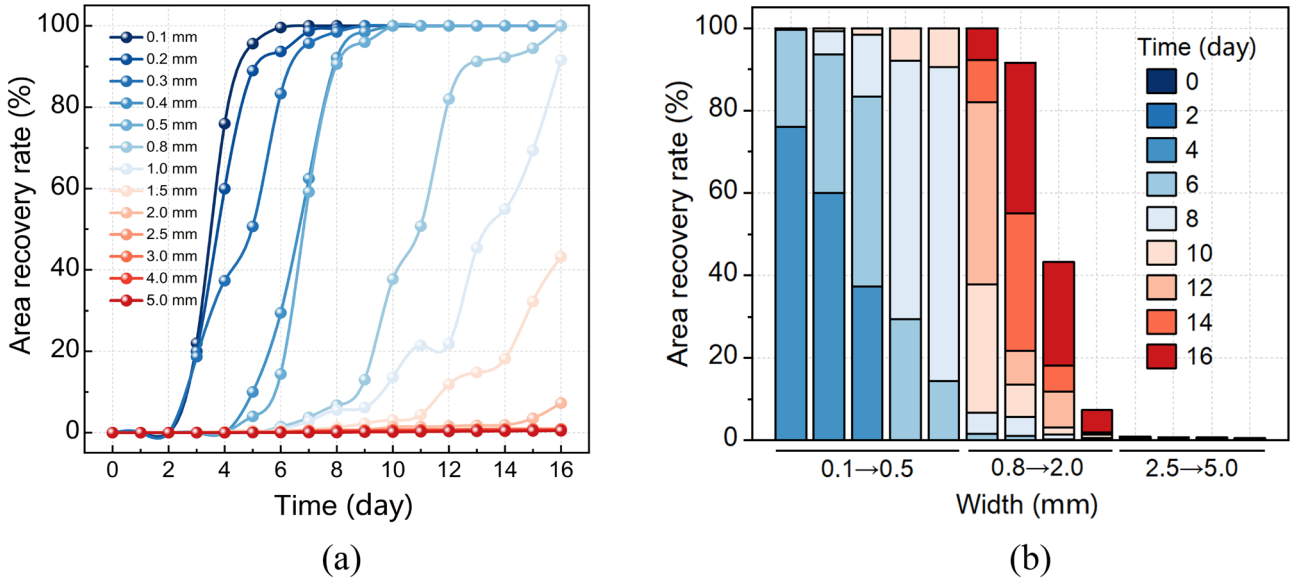

Fig. 6. Crack area repair rate at different repair cycles/crack widths.

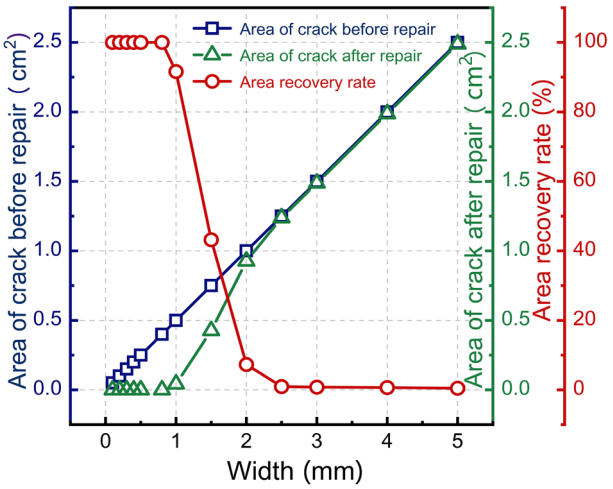

Fig. 7. Comparison of crack area repair rate before and after MICP repair.

when when the area repair rate of the fitted surface corresponding to different widths/repair days is > 100%, i.e., the area repair rate is taken to be 100%).

Analysis of permeability

The variation curves depicting the recovery rate of the permeability coefficient of concrete cracks, categorized by different crack widths and repair durations, are depicted in Fig. 9. The analysis indicates that the permeability coefficients across all specimen groups exhibited a gradual decline with the extension of the repair period. This phenomenon can be primarily attributed to the extensive and dense precipitation of $CaCO_3$ within the cracks. These precipitates not only occluded the voids present in the cracks but also facilitated the formation of a relatively continuous and robust barrier layer through the growth and interconnection of their crystalline structures. This barrier layer effectively obstructs the pathways for water molecule penetration, thereby significantly reducing the permeability coefficient of the concrete. Additionally, as the repair cycle is extended, the accumulation of $CaCO_3$ precipitation leads to an increase in both the thickness and density of the barrier layer, which further enhances its impermeability.

It is important to highlight that the width of cracks significantly impacts the effectiveness of repair interventions[10]. By integrating the results of the previous section and the data in Fig. 9, for narrower cracks (0.1~0.8 mm), the limited spatial dimensions allow for the rapid and uniform precipitation of $CaCO_3$, which effectively fills the entire crack and forms a dense repair layer during the repair cycle. Consequently, the reduction rate of the permeability coefficient can reach 99.4% or higher. In contrast, for cracks with widths between 1.0

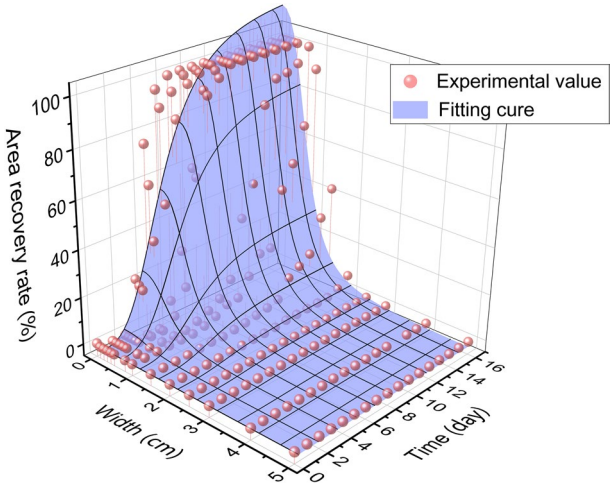

Fig. 8. Fitting surface of area repair rate corresponding to different width / repair times.

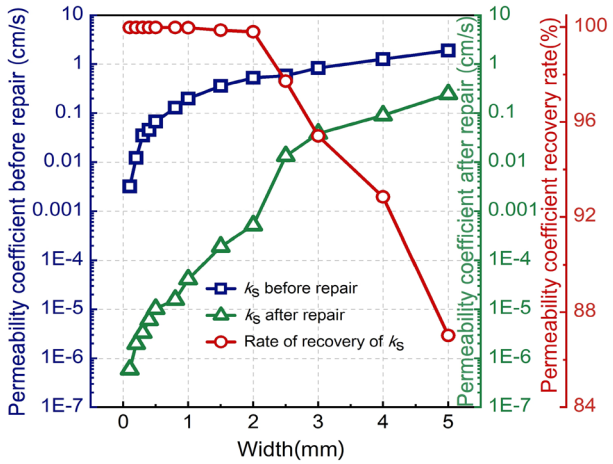

Fig. 9. Comparison of reduction rates of permeability coefficients of cracks before and after MICP repairs.

and 2.0 mm, although the area repair rate is suboptimal, $CaCO_3$ can still create an effective filling in the central region of the crack. This filling can withstand water pressure and contribute to a reduction in the permeability coefficient during permeability testing, the permeability coefficient of the repaired samples was reduced by about three orders of magnitude, the results are similar to the results of penetration experiments by Choi et al.[22], who used MICP to repair mortar cracks with widths ranging from 0.15 to 1.64 mm in 21 immersions.

The results showed that the permeability coefficient of the repaired samples was reduced by about three orders of magnitude compared to the unrepaired samples. However, when the crack width exceeds 2.0 mm, $CaCO_3$ generated at the base of the crack tends to form looser connections, making it challenging to establish a continuous, dense, impermeable layer. Under the pressure exerted by the water head, $CaCO_3$ connections in the central region are particularly vulnerable to erosion and damage, leading to a marked decrease in the recovery rate of permeability coefficient. When the crack width ranges from 0.1 to 2.0 mm, the recovery rate of permeability coefficient remains nearly constant, exceeding 99%. However, for cracks wider than 2.0 mm, a sharp decline in the recovery rate is observed. Specifically, for cracks with a width of 5.0 mm, after 16 repair cycles, the recovery rate of permeability coefficient only reaches 87%. This indicates that the stability of $CaCO_3$ precipitation is not solely dependent on the amount of deposition, but is also closely linked to its spatial distribution and the strength of its interconnections within the cracks.

Waterproof performance analysis

In this study, twelve sets of specimens exhibiting typical cracking patterns were selected for analysis. The relationship between the accumulated capillary water absorption height (i) and the square root of time ($t^{1/2}$) over a 48-h period is illustrated in Fig. 10. The experimental results in Fig. 10 indicate that i of concrete cracks increases as the width of the cracks increases. This observation suggests that narrower cracks impede the flow of water molecules due to factors such as surface tension and friction, which hinders the rapid penetration of water

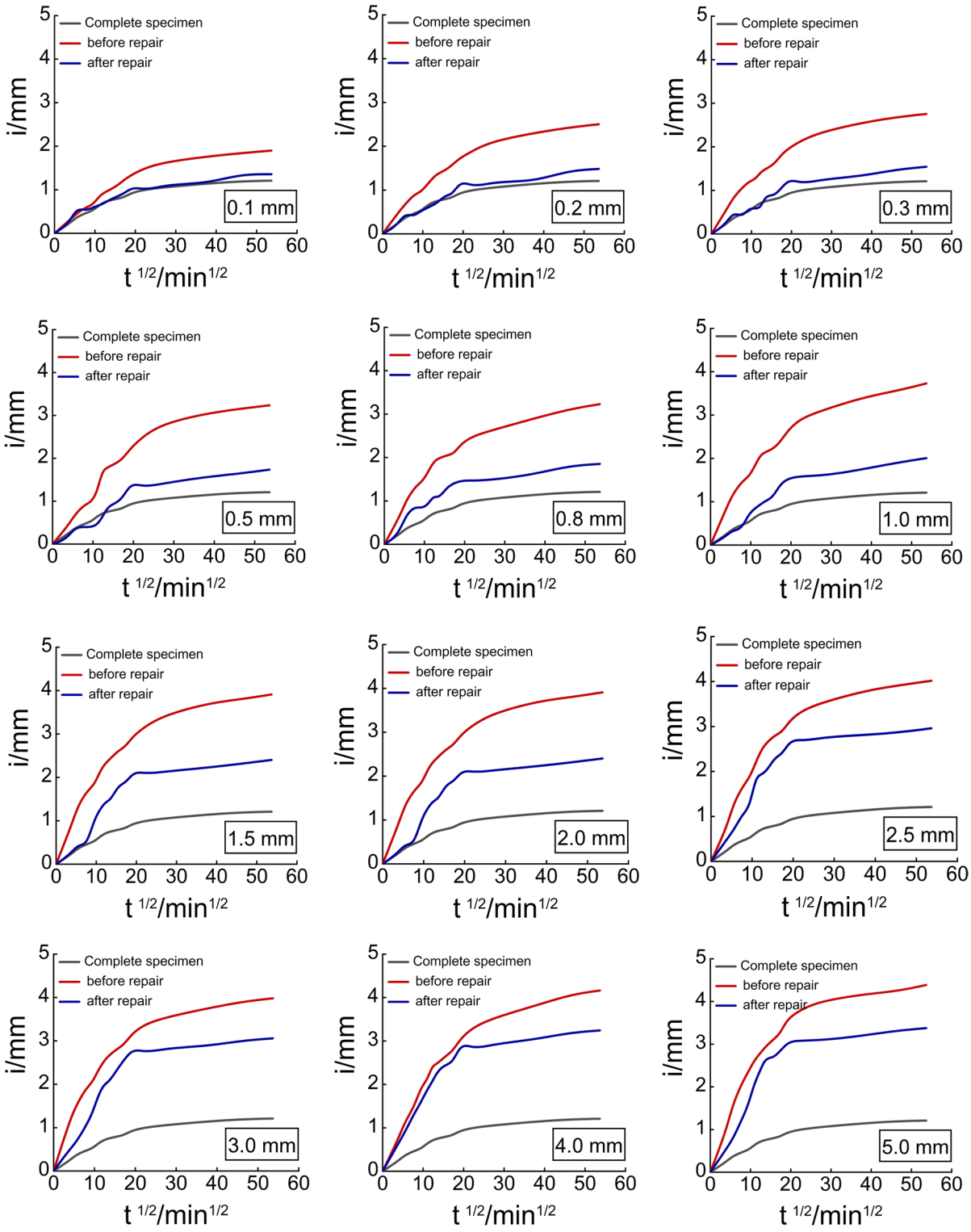

Fig. 10. Cumulative water absorption curves for typical width cracks.

into the interior of the concrete. Conversely, wider cracks facilitate the movement of water by providing more expansive channels, thereby reducing these impediments and allowing for a more rapid penetration of water, which in turn enhances the capillary water absorption rate within the cracks.

To more intuitively demonstrate the changes in capillary water absorption height before and after the application of the MICP technique for crack repair, Fig. 11 presents a bar chart showing the capillary water absorption heights of cracks with various widths both before and after repair, as well as the percentage reduction in capillary water absorption height after repair.

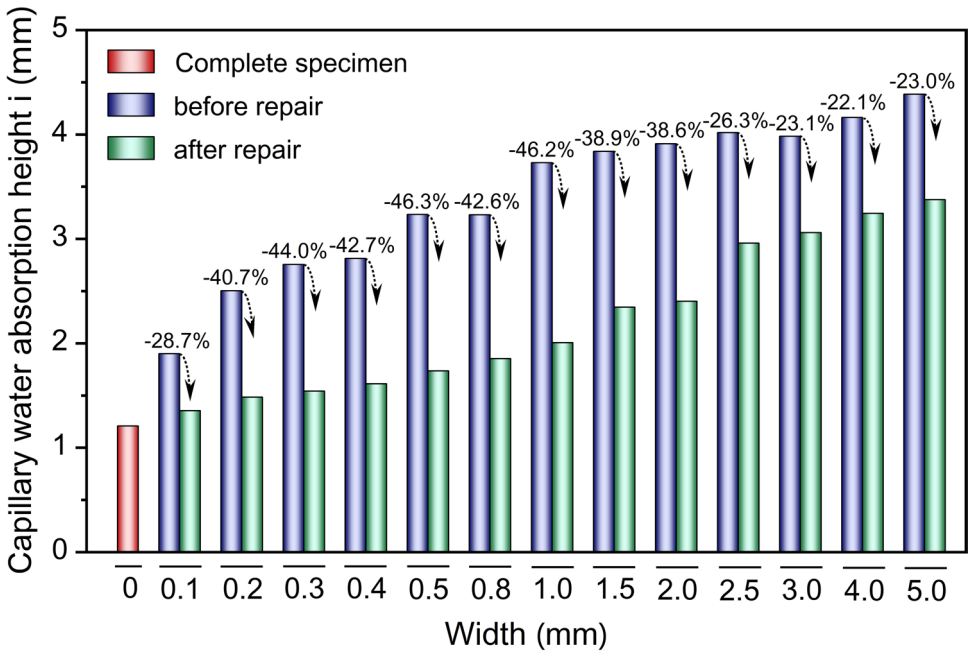

Fig. 11. Comparison of capillary absorption heights before and after MICP repair.

Following the application of MICP technique, the capillary water absorption of the concrete specimens exhibited a marked reduction. This phenomenon can be attributed to the extensive filling and curing of $CaCO_3$ crystals that are produced during MICP process within the cracks. These $CaCO_3$ crystals serve a dual purpose: they not only occupy the voids within the cracks and establish a dense protective layer that effectively prevents external water from making direct contact with the interior of the concrete, but they also significantly decrease the capillary pores of the concrete specimens that are subjected to water exposure. This reduction in pore size further limits the pathways available for water penetration. Collectively, these mechanisms contribute to a substantial decrease in the capillary water absorption rate of the repaired concrete cracks.

At the same time, the cumulative capillary water absorption height of each crack specimen exhibited an almost linear increase with time during the initial phase ($t < 6$ h), followed by a transition into a second phase characterized by slow linear growth. This alteration in the growth rate may be attributed to the fact that, at later stages, moisture encounters smaller gel pores rather than capillary pores, thereby increasing the resistance to moisture penetration and subsequently reducing the capillary water absorption rate. Furthermore, Martys and Ferraris[42] also pointed out the sub-stable state of the air–water interface formed within the pores may also act as a barrier to further water penetration, representing another significant factor affecting the time-dependent behavior of capillary water absorption.

Figure 12 shows the effectiveness of MICP in repairing cracks varies with the width of the cracks. Specifically, for cracks within the 0.1~1.0 mm range, the relatively narrow space facilitates the formation of a "bridging" effect by $CaCO_3$ particles, allowing them to accumulate more densely and form a robust repair layer. Consequently, the repair effectiveness is maximized, with a waterproofing performance enhancement of up to 78.2%, Jongvivatsakul et al.[23] used bacterial and urea solutions to repair cracked mortar with a width of 0.4 mm over a period of 20 days. They found that the water absorption of cracked mortar samples treated with MICP decreased by almost 72%, the reduction in water absorption was similar to that measured in this paper, and the main error was due to the difference in material between concrete and mortar. In contrast, for cracks exceeding 1.0 mm in width, while MICP technology can still yield certain improvement in waterproofing performance (for instance, a 25.2% enhancement for a crack width of 5.0 mm), the overall repair effect is considerably decreased. This limitation is primarily attributed to the increased crack width, which hinders the effective accumulation of $CaCO_3$ particles within the crack, thereby adversely affecting the densification and integrity of the repair layer.

Composition and morphology analysis of the generated material

A specimen exhibiting an initial crack width of 1.0 mm was utilized as a case study to compare and analyze the composition and morphology of the material within the crack prior to and following MICP repair. Figure 13a,b presents XRD patterns of the materials located in the cracks of the specimen both before repair and after MICP treatment, maintaining the initial crack width of 1.0 mm. Figure 14a,b presents SEM images of the material located within the crack of the specimen, which initially exhibited a crack width of 1.0 mm, following MICP repair process.

In Fig. 13a,b, the materials present within the cracks of the unrepaired specimens predominantly consist of typical components found in cementitious materials, such as SiO_2 and a minor quantity of $CaCO_3$, where the 2θ position of the diffraction peak of SiO_2 is about 26.7°. In contrast, the XRD pattern of the concrete specimens repaired by MICP showed that the calcite ($CaCO_3$) peak at 29.4°(2θ) was significantly enhanced, indicating

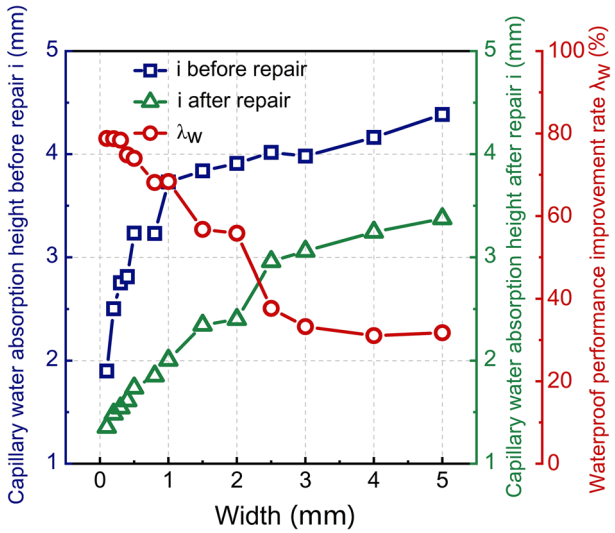

Fig. 12. Waterproofing performance enhancement factor for each crack.

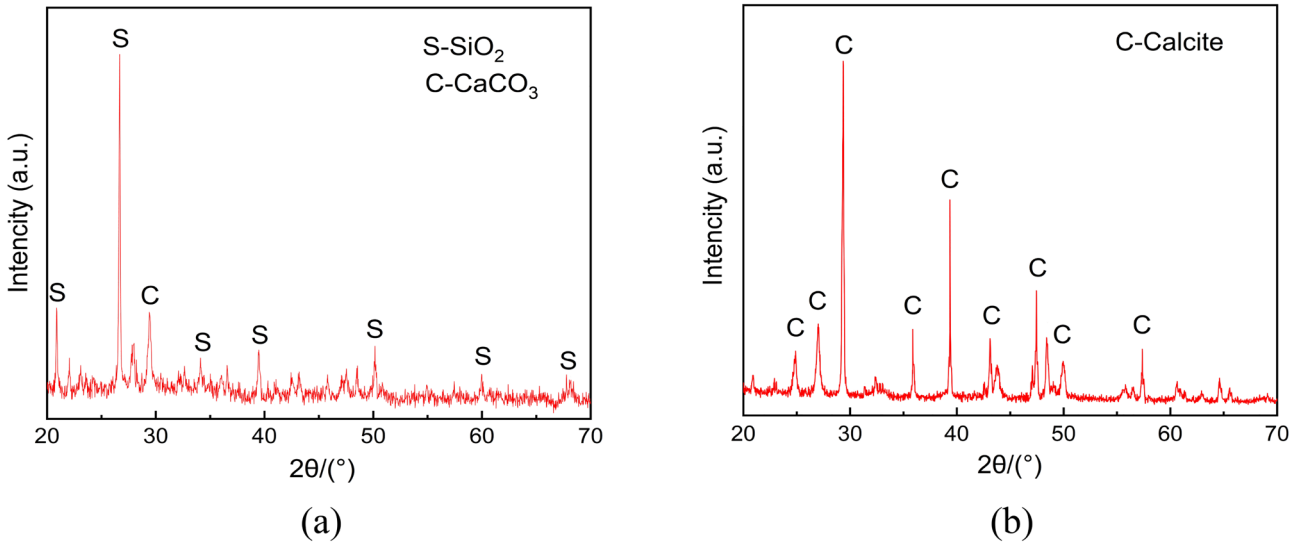

Fig. 13. The XRD patterns of internal materials of cracks before and after MICP repair.

that the material formed in the repaired cracks was mainly calcite, which was a specific form of $CaCO_3$. This observation further confirms that the fracture repair is achieved by the deposition of $CaCO_3$ in the fracture, which is consistent with the results of other researchers[43,44].

The analysis of SEM images in Fig. 14a,b reveals that the internal products of unrepaired concrete cracks manifest as stacked flakes or snowflake-like structures when observed under an electron microscope. This phenomenon occurs due to the generation of positively charged C–S–H gel at the inner walls of the cracks during the hydration reaction of cement in the presence of water, the similar results were found in the study of Alghamri et al.[45]. In contrast, concrete cracks that have been repaired using MICP exhibit a different behavior. The negatively charged CO_3^{2-} present in the cell wall are readily attracted to the positively charged Ca^{2+} associated with C–S–H gel, which becomes adsorbed onto the inner walls of the cracks. Subsequently, a significant quantity of positively charged Ca^{2+} in the cementing solution reacts within the cracks, facilitating the formation of substantial amounts of $CaCO_3$ precipitates. As the repair process continues over time, these $CaCO_3$ particles aggregate and effectively fill the cracks. It further indicates that the majority of $CaCO_3$ deposits within the cracks exhibit either regular or irregular elliptical shapes, which contribute to the filling of the cracks, Diego et al.[46] and Wang et al.[47] analyzed in detail the formation mechanism of elliptical calcite crystals in the process of microbially induced calcium carbonate precipitation (MICP) and found that this phenomenon is driven by the induction of microbial metabolites, crystallization kinetics and thermodynamics, and a non-classical crystallization mechanism. Microbial metabolites (such as ammonia and carbonate ions produced by the urease decomposition of urea) provide the raw materials for calcite precipitation and guide crystal growth. Spherical

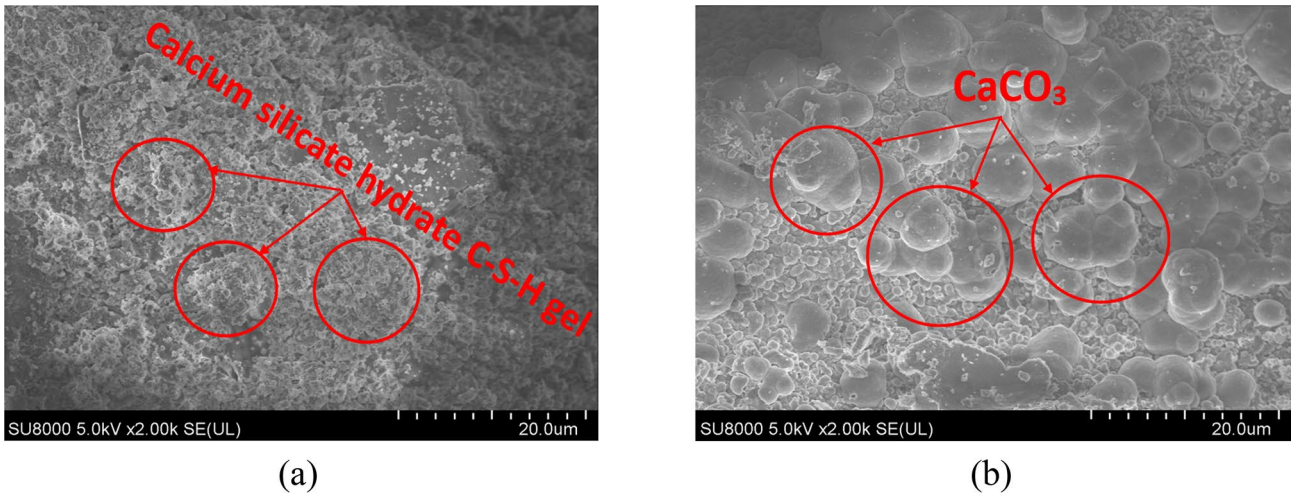

Fig.14. The microscopic SEM structure of the material inside the cracks before and after MICP repair.

crystals are energetically favorable because they minimize surface energy and maintain stability. Amorphous calcium carbonate (ACC) first transforms into nanoparticles, which then aggregate into spherical crystals through a non-classical particle attachment mechanism, facilitating the filling and stabilization of cracks. It can be inferred that the enhancement of impermeability and waterproofing in the cracked concrete specimens repaired through MICP is primarily due to the successive deposition of $CaCO_3$ within the cracks, which serves as a solid barrier and overlaying film.

In summary, following 16 cycles of MICP for the repair of cracks in desert channel linings, when the width of concrete cracks exceeds 0.8 mm, the area repair rate of MICP technology begins to decline significantly due to physical space limitations. Furthermore, when the width of the cracks exceeds 2.0 mm, the insufficient bond strength of $CaCO_3$ at the bottom of the specimen can lead to erosion and subsequent destruction, resulting in a marked decrease in the permeability coefficient recovery rate. Additionally, when the width of the cracks exceeds 1.0 mm, the top of the specimen is adversely affected by the width, leading to a substantial decline in both density and integrity, which in turn affects the capillary absorption recovery rate. Therefore, to ensure the stable operation of the open channels in Xinjiang Desert while maintaining the apparent integrity of the cracks and achieving optimal waterproofing and impermeability, a $Width_0$ of 1.0 mm for concrete cracks was determined for the 16-cycle MICP repair. This approach not only ensures effective crack repair but also mitigates the risk of adversely affecting the normal operation of the desert channels due to excessively prolonged repair cycles.

Conclusions

(1) **Strain cultivation and optimization of mineralization:** To address the problem of lining cracking of open channel bank slope in the Xinjiang desert, this study applied microbial—induced calcium carbonate precipitation (MICP) repair technology. *Sporosarcina pasteurii* was selected as the functional strain. Strain activity was regulated through strain resuscitation in solid medium, liquid—phase amplification, and urease activity monitoring. Considering the characteristics of bacterial growth and the Xinjiang desert environment, orthogonal tests were first carried out. Then, Pearson correlation analysis was employed to screen suitable microbial culture conditions and optimize the influencing factors of mineralization. These efforts aimed to provide a reference strategy for MICP technology to repair the lining cracks of open channels in the Xinjiang desert.

(2) **Macro-and micro-level evaluation of repair efficiency:** Based on macroscopic and microscopic tests, the effect of MICP technology on repairing lining cracks was evaluated. Lining cracks of different widths were prefabricated using the steel plate insertion and extraction method, and 16 cycles of repair were carried out using the injection method. Macroscopic tests, including area repair rate, constant head permeability test, and capillary water absorption test, were conducted. Combined with microscopic characterization (XRD mineral diffraction and SEM scanning electron microscopy), the effect of MICP technology on repairing lining cracks of bank slopes was evaluated from a macro–micro perspective. Additionally, the critical width of MICP technology for repairing lining cracks of bank slopes within the specified repair period was determined.

(3) **Proposed repair strategy:** For concrete cracks larger than the critical width, it is recommended to use the local aeolian soil from the desert open channel as aggregate in the later stage, combined with MICP technology for repair. This approach not only enhances the environmental adaptability of the repair material but also reduces costs and improves repair efficiency. Meanwhile, considering that this study has focused on the open channel in the Xinjiang desert for targeted repair research, and in order to further enhance the generalizability of the research method, it is recommended that researchers working on similar water conveyance projects refer to the repair methods proposed in this study. Considering that the lining strength

and thickness may vary among different projects, they should appropriately adjust the repair parameters, timing, and methods according to the specific characteristics of their projects, in order to provide practical and feasible reference suggestions for the long-term operation and maintenance of similar water conveyance projects.

Data availability

Data is provided within the manuscript or supplementary information files.

Received: 4 March 2025; Accepted: 7 May 2025
Published online: 15 May 2025

References

1. Chu, H. Q., Liang, Y. C., Guo, M. Z., Zhu, Z. Y. & Zhao, S. J. Effect of electro-deposition on repair of cracks in reinforced concrete. *Constr. Build. Mater.* **238**, 117725 (2020).
2. Xi, B., Salam, A. O. & Liberato, F. Effect of different environments on the self-healing performance of Ultra high-performance concrete—A systematic literature review. *Constr. Build. Mater.* **374**, 130946 (2023).
3. Fadi, A. et al. Physical, strength, durability and microstructural analysis of self-healing concrete: A systematic review. *Case Stud. Constr. Mater.* **18**, e01730 (2023).
4. Lu, C. H., Li, Z. H., Wang, J. H., Zheng, Y. L. & Cheng, L. An approach of repairing concrete vertical cracks using microbially induced carbonate precipitation driven by ion diffusion. *J. Build. Eng.* **73**, 106798 (2023).
5. Zhao, C. et al. Influence of injection methods on bio-mediated precipitation of carbonates in fracture-mimicking microfluidic chip. *Géotechnique.* **75**(2), 153–165 (2025).
6. Ma, G. L. et al. Strength and permeability of bentonite-assisted biocemented coarse sand. *Can. Geotech. J.* **58**(7), 969–981 (2021).
7. Xiao, Y. et al. Compression behavior of MICP-treated sand with various gradations. *Acta Geotech.* **16**(5), 1391–1400 (2021).
8. Miao, L. C., Wang, H. X., Sun, X. H., Wu, L. Y. & Fan, G. C. Effect analysis of biomineralization for solidifying desert sands. *Biogeotechnics.* **2**(1), 100065 (2025).
9. Meng, H., Gao, Y. F., He, J., Qi, Y. S. & Hang, L. Microbially induced carbonate precipitation for wind erosion control of desert soil: Field-scale tests. *Geoderma* **383**, 114723 (2021).
10. Tittelboom, K. V., Belie, N. D., Muynck, W. D. & Verstraete, W. Use of bacteria to repair cracks in concrete. *Cem. Concr. Res.* **40**(1), 157–166 (2010).
11. Muynck, W. D., Debrouwer, D., Belie, D. N. & Verstraete, W. Bacterial carbonate precipitation improves the durability of cementitious materials. *Cem. Concr. Res.* **38**(7), 1005–1014 (2008).
12. Cuthbert, M. O., McMillan, L. A., Handley-Sidhu, S., Riley, M. S. & Tobler, D. J. A field and modeling study of fractured rock permeability reduction using microbially induced calcite precipitation. *Environ. Sci. Technol.* **47**(23), 13637–13643 (2013).
13. Khaliq, W. & Ehsan, M. B. Crack healing in concrete using various bio influenced self-healing techniques. *Constr. Build. Mater.* **102**, 349–357 (2016).
14. Achal, V., Mukherjee, A., Basu, P. C. & Reddy, M. S. Strain improvement of Sporosarcina pasteurii for enhanced urease and calcite production. *J. Ind. Microbiol. Biot.* **36**(7), 981–988 (2009).
15. Lu, C. H., Bu, S. Z., Shahin, M. A., Zheng, Y. L. & Cheng, L. Mitigation of alkali-silica reaction by microbially induced $CaCO_3$ protective layer on aggregates. *Constr. Build. Mater.* **328**, 127065 (2022).
16. Jiang, L., Xia, H., Wang, W. J., Zhang, Y. & Li, Z. Applications of microbially induced calcium carbonate precipitation in civil engineering practice: A state-of-the-art review. *Constr. Build. Mater.* **404**, 133227 (2023).
17. Mohd, B. A. et al. Assessment of the mechanical and durability characteristics of bio-mineralized Bacillus subtilis self-healing concrete blended with hydrated lime and brick powder. *Case Stud. Constr. Mater.* **19**, e02672 (2023).
18. Achal, V., Mukerjee, A. & Sudhakara, R. M. Biogenic treatment improves the durability and remediates the cracks of concrete structures. *Constr. Build. Mater.* **48**, 1–5 (2013).
19. Wiktor, V. & Jonkers, H. M. Quantification of crack-healing in novel bacteria-based self-healing concrete. *Cem. Concr. Comp.* **33**(7), 763–770 (2011).
20. Tziviloglou, E., Wiktor, V., Jonkers, H. M. & Schlangen, E. Bacteria-based self-healing concrete to increase liquid tightness of cracks. *Constr. Build. Mater.* **122**, 118–125 (2016).
21. Wang, J. Y., Belie, N. D. & Verstraete, W. Diatomaceous earth as a protective vehicle for bacteria applied for self-healing concrete. *J. Ind. Microbiol. Biot.* **39**(4), 567 (2012).
22. Choi, S. G., Wang, K. J., Wen, Z. Y. & Chu, J. Mortar crack repair using microbial induced calcite precipitation method. *Cem. Concr. Comp.* **83**, 209–221 (2017).
23. Jongvivatsakul, P., Janprasit, K., Nuaklong, P., Pungrasmi, W. & Likitlersuang, S. Investigation of the crack healing performance in mortar using microbially induced calcium carbonate precipitation (MICP) method. *Constr. Build. Mater.* **212**, 737–744 (2019).
24. Huang, H. J., Du, C. B., Yi, F., Wang, M. & Lv, Z. Q. Enhancing concrete crack healing: Revealing the synergistic impacts of multicomponent microbial repair systems. *Case Stud. Constr. Mater.* **21**, e03402–e03402 (2024).
25. Fan, L., Zheng, J. H., Peng, S. Q., Xun, Z. Z. & Chen, G. L. Experimental investigation on the influence of crack width of asphalt concrete on the repair effect of microbially induced calcite precipitation. *Materials.* **16**(9), 3576 (2023).
26. Whiffin, V.S. Microbial $CaCO_3$ Precipitation for the production of biocement, Murdor University Repository, PhD 1–162 (2004).
27. GB 50010, Code for Design of Concrete Structures (2015 version), China Architecture and Building Press, Beijing, China, (2015).
28. Zhu, J. N., Wang, J. X. & Feng, C. M. Deformation characteristics and sensitivity analysis of aeolian soil bank slope in Xinjiang desert open channel. *Environ. Earth. Sci.* **83**(14), 1–16 (2024).
29. Tomczak, K. & Jakubowski, J. The effects of age, cement content, and healing time on the self-healing ability of high-strength concrete. *Constr. Build. Mater.* **187**, 149–159 (2018).
30. GBT 50081 2019, Standard test method for physical and mechanical properties of concrete (2019 version), China Academy of Architectural Engineering, Beijing, China, (2019).
31. Ding, X. Q. et al. Capillary water absorption and micro pore connectivity of concrete with fractal analysis. *Crystals* **10**(10), 892 (2020).
32. Junwale, R., Nikode, A., Bhutange, S. & Latkar, M. V. Crack healing in cement mortar using enzyme induced calcium carbonate precipitation. *Constr. Build. Mater.* **394**, 132223 (2023).
33. Mitchell, J. K. & Santamarina, J. C. Closure to "Biological Considerations in Geotechnical Engineering" by James K. Mitchell and J. Carlos Santamarina. *J. Geotech. Geoenviron.* **133**(4), 486–486 (2007).
34. DeJong, T. J., Mortensen, M. B., Martinez, C. B. & Nelson, C. D. Bio-mediated soil improvement. *Ecol. Eng.* **36**(2), 197–210 (2008).
35. Algaifi, H. M. et al. Insight into the role of microbial calcium carbonate and the factors involved in self-healing concrete. *Constr. Build. Mater.* **254**, 119258 (2020).
36. Sivakumar, G., Moeka, Y., Kazunori, N., Volodymyr, I. & Satoru, K. Calcium phosphate biocement using bone meal and acid urease: An eco-friendly approach for soil improvement. *J. Clean Prod.* **319**, 128782 (2021).

37. Feng, Z. Y., Zhao, Y. X., Zeng, W. L., Lu, Z. M. & Shah, S. P. Using microbial carbonate precipitation to improve the properties of recycled fine aggregate and mortar. *Constr. Build. Mater.* **230**, 116949 (2020).
38. Peng, S. Q., Di, H., Fan, L., Fan, W. & Qin, L. Factors affecting permeability reduction of MICP for fractured rock. *Front. Earth. Sci.* https://doi.org/10.3389/feart.2020.00217 (2020).
39. Chek, A., Crowley, R., Ellis, T., Durnin, M. & Wingender, B. Evaluation of factors affecting erodibility improvement for MICP-treated beach sand. *J. Geotech. Geoenviron.* https://doi.org/10.1061/(ASCE)GT.1943-5606.0002481 (2021).
40. Wu, M. Y., Hu, X. M., Zhang, Q., Xue, D. & Zhao, Y. Y. Growth environment optimization for inducing bacterial mineralization and its application in concrete healing. *Constr. Build. Mater.* **209**, 631–643 (2019).
41. Kalhori, H. & Bagherpour, R. Application of carbonate precipitating bacteria for improving properties and repairing cracks of shotcrete. *Constr. Build. Mater.* **148**, 249–260 (2017).
42. Martys, N. & Ferraris, C. Capillary transport in mortars and concrete. *Cem. Concr. Res.* **27**(5), 747–760 (1997).
43. Luo, M., Qian, C. X. & Li, R. Y. Factors affecting crack repairing capacity of bacteria-based self-healing concrete. *Constr. Build. Mater.* **87**, 1–7 (2015).
44. Feng, J. H., Su, Y. L. & Qian, C. X. Coupled effect of PP fiber, PVA fiber and bacteria on self-healing efficiency of early-age cracks in concrete. *Constr. Build. Mater.* **228**, 116810 (2019).
45. Alghamri, R. & Al-Tabbaa, A. Self-healing of cracks in mortars using novel PVA-coated pellets of different expansive agents. *Constr. Build. Mater.* **254**, 119254 (2020).
46. Diego, J. R. et al. The kinetics and mechanisms of amorphous calcium carbonate (ACC) crystallization to calcite, via vaterite. *Nanoscale* **3**(1), 265–271 (2011).
47. Wang, Q. H. et al. Stabilization and crystallization mechanism of amorphous calcium carbonate. *J. Colloid Interf Sci.* **680**(PB), 24–35 (2025).

Acknowledgements

The authors would like to acknowledge the financial support from Natural Science Foundation of Xinjiang Uygur Autonomous Region (No. 2024D01A73) and Open Research Topics of Xinjiang Key Laboratory of Hydraulic Engineering Security and Water Disasters Prevention for 2024(No. ZDSYS-JS-2024-10).

Author contributions

J.W. contributed to conceptualization, funding acquisition, methodology, project administration, supervision, and writing-review & editing. J.Z. was responsible for investigation, experiments, and writing the original draft. Y.L., S.Z., and C.F. all participated in conceptualization, writing the original draft, and writing-review & editing. All authors reviewed the manuscript.

Declarations

Competing interests

The authors declare no competing interests.

Additional information

Correspondence and requests for materials should be addressed to J.W.

Reprints and permissions information is available at www.nature.com/reprints.

Publisher's note Springer Nature remains neutral with regard to jurisdictional claims in published maps and institutional affiliations.